Acta Crystallographica Section B
Structural Science
ISSN 0108-7681

The incommensurately modulated crystal structure of β-Pb_2BiVO_6: interpretation of the phase transition $\alpha \rightarrow \beta \rightarrow \delta$ and conduction properties of related materials

Pascal Roussel,[a]* Olfa Labidi,[a,b] Marielle Huve,[a] Michel Drache,[a] Jean-Pierre Wignacourt[a] and Vaclav Petricek[b]

[a]Unité de Catalyse et de Chimie du Solide, CNRS UMR 8181 (Equipe de Chimie du Solide), ENSCL, USTL-59655 Villeneuve D'Ascq CEDEX, France, and [b]Institute of Physics, ASCR v.v.i., Na Slovance 2, 182 21 Praha 8, Czech Republic

Correspondence e-mail: pascal.roussel@ensc-lille.fr

Received 13 November 2008
Accepted 2 June 2009

A new polymorph of Pb_2BiVO_6 was prepared under ambient conditions and its crystal structure was determined by single-crystal X-ray diffraction. The phase transitions $\alpha \rightarrow \beta$ and $\beta \rightarrow \delta$ were identified in the mother phase; the high-temperature form δ-Pb_2BiVO_6 eventually decomposes at 753 K to a mixture of Pb_4BiVO_8 and the high-temperature form of $PbBiVO_5$ before showing recombination at 923 K. β-Pb_2BiVO_6 has an incommensurate monoclinic modulated structure. This crystal structure is twinned and complementary structural investigations of a powder sample of β-Pb_2BiVO_6 by TEM diffraction studies confirmed the lattice and incommensurate modulation character. Log $\sigma = f(T^{-1})$ dependences for Pb_2BiVO_6-related materials (6% *M*-for-V-substituted compositions; *M* = Cr, Mn, P) are reported, which allow the characterization (E_a and isothermal σ values) of the β- as well as the δ- and α-Pb_2BiVO_6 varieties.

1. Introduction

Pb_2BiVO_6 was shown to have several polymorphic forms labelled α to δ (Mizrahi, Wignacourt *et al.*, 1995; Mizrahi, Huve *et al.*, 1995; Mizrahi, 1996; Mizrahi *et al.*, 1997; Giraud *et al.*, 1999, 2001). The α phase is obtained by air quenching of a stoichiometric reaction product from 973 K. The thermal evolution of α shows (DTA, HTXRD) four modifications: $\alpha \rightarrow \beta \rightarrow \delta \rightarrow \gamma \rightarrow \delta$. On cooling, only the $\delta \rightarrow \alpha$ phase transition is observed. The γ form has been shown recently to be a mixture of Pb_4BiVO_8 and of the high-temperature, monoclinic form of $PbBiVO_5$ (Mizrahi *et al.*, 1997).

α-Pb_2BiVO_6 is monoclinic (Radosavljevic Evans *et al.*, 2001; see Table 1); O atoms are in tetrahedral interstices formed by four Bi and Pb atoms. These tetrahedra were joined by Bi–Bi edge-sharing in two dimensions to form ($O_2Bi_2Pb_4$) dimers, associated with Bi–Pb edge-sharing in infinite ribbons parallel to the *b* axis. Mixed $O(V,Bi,Pb)_4$ tetrahedra bridge the $O(Bi,Pb)_4$ ribbons by edge-sharing, to complete the three-dimensional nature of the structure.

δ-Pb_2BiVO_6 is orthorhombic (Radosavljevic Evans *et al.*, 2002); the structure is built out of OBi_2Pb_2 tetrahedra, forming dimers by sharing Bi–Bi edges, then tetramers by sharing Bi–Pb edges, which develop infinite two-dimensional ribbons along the [010] direction.

In recent work (Labidi *et al.*, 2005) direct phase transitions $\alpha \rightarrow \beta \rightarrow \delta$ and $\alpha \rightarrow \delta$ were identified in P-for-V-substituted $Pb_2Bi(V_{1-x}P_x)O_6$ solid solutions, when $x \geq 0.10$, thus avoiding the intermediate decomposition of the high-temperature δ form noticed in the δ-Pb_2BiVO_6 mother phase. With several tentative substitutions for V, new polymorphs are observed: α'-$Pb_2BiV_{1-x}Mn_xO_{6-y}$ ($x = 0.06$) which is monoclinic (Labidi *et al.*, 2004). Under a slow cooling process, the

Table 1
Polymorphic forms of Pb_2BiVO_6.

Polymorph	Symmetry	Space group	Cell parameters
α^a	Monoclinic	Pn	$a = 7.717$ (3), $b = 5.845$ (3), $c = 29.081$ (8) Å, $\beta = 94.27$ (1)°
β^b	Monoclinic	$P2_1/m(0\beta0)s0$ (3 + 1)-dimensional approach	$a = 15.0501$ (5), $b = 5.9011$ (3), $c = 7.5322$ (5) Å, $\beta = 101.57$ (2)° $\mathbf{q} = 0.2338$ (3)$\mathbf{b}^*$
δ^a	Orthorhombic	$Pmcn$	$a = 6.03828$ (1), $b = 9.44267$ (2), $c = 12.07438$ (4) Å
α'-$Pb_2BiV_{1-x}Mn_xO_{6-y}$ ($x = 0.06$)^c	Monoclinic	$P2_1/m$	$a = 7.684$ (3), $b = 5.822$ (3), $c = 14.708$ (6) Å, $\beta = 100.92$ (1)°
δ'-$Pb_2Bi(V_{1-x}P_x)O_6{}^d$	Orthorhombic	$Pbca$	$a = 5.922$ (1), $b = 18.395$ (5), $c = 11.864$ (3) Å

References: (*a*) Radosavljevic Evans *et al.* (2001); (*b*) this work; (*c*) Labidi *et al.* (2004); (*d*) Labidi *et al.* (2005).

Table 2
Crystal data and structure refinement for β-Pb_2BiVO_6 at room temperature.

Crystal data	
Chemical formula	Pb_2BiVO_6
M_r	770.3
Crystal system, space group	Monoclinic, $P2_1/m(0\beta0)s0$
Temperature (K)	298
a, b, c (Å)	15.0501 (5), 5.9011 (3), 7.5322 (5)
β (°)	101.57 (2)
Modulation wavevector	$\mathbf{q} = 0.2338$ (3)$\mathbf{b}^*$
V (Å^3)	655.37 (8)
Z	4
Radiation type	Mo $K\alpha$
μ (mm^{-1})	0.71073
Crystal form, size	Platelet, 0.21 × 0.12 × 0.05
Data collection	
Diffractometer	Bruker CCD
Data-collection method	ω scans
Absorption correction	Analytical
$T_{\min}$	0.301
$T_{\max}$	1.00
No. of measured, independent and observed reflections	110 335, 24 247, 4097
Criterion for observed reflections	$I > 3\sigma(I)$
$R_{\rm int}$	0.152
$\theta_{\max}$ (°)	40.3
Refinement	
Refinement on	F
$R[F^2 > 2\sigma(F^2)], wR(F^2), S$	0.036, 0.032, 1.07
$(\Delta/\sigma)_{\max}$	< 0.0001
$\Delta\rho_{\max}, \Delta\rho_{\min}$ (e Å^{-3})	3.44, −6.04

$Pb_2Bi(V_{1-x}P_x)O_6$ high-temperature δ-type phase (orthorhombic) transforms into a closely related δ'-$Pb_2Bi(V_{1-x}P_x)O_6$ polymorph ($x \geq 0.15$) which is preserved at room temperature (Labidi *et al.*, 2005). All these polymorphic forms share a common lattice parameter of ~ 5.9 Å, along which are aligned $O(Bi,Pb)_4$ infinite ribbons which constitute the backbone of these structures; each identified polymorph has its own characteristically oriented set of VO_4 tetrahedra surrounding those ribbons.

The single-crystal structure of the intermediate polymorphic variety β-Pb_2BiVO_6 is so far unresolved. With the help of transmission electron-microscope data, and under a novel stabilization thermal cycle, we succeeded in obtaining the β-Pb_2BiVO_6 variety at room temperature, both as powder samples and as single crystals, thus allowing a precise crystal structure investigation.

2. Experimental

Pb_2BiVO_6 was prepared from a mixture of stoichiometric proportions of PbO (Riedel Haën, 99%), Bi_2O_3 (Aldrich, 99.9%) and V_2O_5 (Aldrich, 99.6%) that was held at 973 K for 4 d, and then air-quenched. In order to determine the temperature of the α–β phase transition, this powder was studied as a function of temperature with a D8 Bruker diffractometer equipped with an Anton Paar HTK1200N furnace. The powder was placed in a gold tube, carried to the melting point at 1173 K, and then cooled and held at 1023 K for 50 h, then finally returned to ambient temperature. Under these conditions of preparation we obtained crystals of the α phase. This very same tube was re-treated in the furnace at 703 K (*i.e.* within the range of stability of the β phase), annealed for 10 h, then air-quenched back to room temperature by furnace power disconnection. Blocks of orange crystals were obtained and broken. A crystal suitable for data collection was selected and single-crystal X-ray diffraction intensities were measured on a Bruker APEX2 CCD 4 K diffractometer, Mo $K\alpha$ radiation, under the experimental conditions shown in Table 2.[1]

Electron-diffraction patterns (EDP) were obtained on a Philips CM30 transmission electron microscope equipped with a precession system. The material was crushed and dispersed on a holey carbon film deposited on a Cu grid.

An impedance spectroscopy investigation was performed on material pellets (5 mm in diameter, 2–3 mm in thickness) sintered at 1123 K for 48 h, which allowed ~ 90% material densification. Gold electrodes were deposited on both faces of each pellet, by sputtering. The sample impedance was measured (1–106 Hz) in an open cell working in static air, using a Schlumberger 1170 frequency response analyser. Each measurement (step: 10 K) was realized after 1 h temperature stabilization, which is usually sufficient to obtain the thermodynamic equilibrium for oxide-containing phases. The evolution of the material conductivity *versus* temperature was

---

[1] Supplementary data for this paper are available from the IUCr electronic archives (Reference: BP5019). Services for accessing these data are described at the back of the journal.

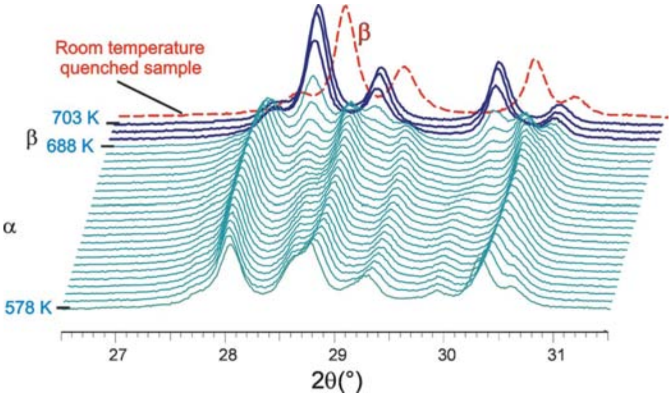

Figure 1
High-temperature X-ray diffraction evolution of Pb_2BiVO_6 from 578 to 703 K showing the transformation of α into β. The red diffraction curve is obtained after quenching at room temperature. The blue curve presents β-Pb_2BiVO_6 after the quenching. This figure is in colour in the electronic version of this paper.

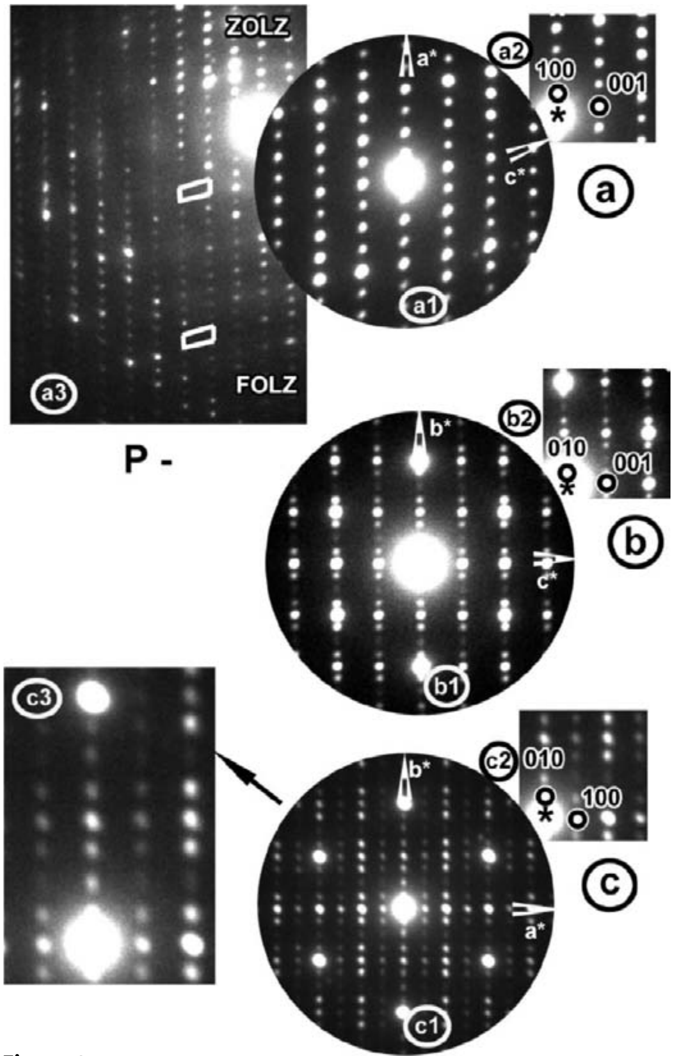

Figure 2
(*a*) [010], (*b*) [100], (*c*) [001] zone-axis patterns; (*a*1) ZOLZ (*a*2) enlargement of Fig. (*a*1); (*a*3) comparison between [FOLZ] and [ZOLZ] indicating neither a shift nor a difference in periodicity. (*b*1) ZOLZ (*b*2) enlargement of Fig. (*b*1); (*c*1) ZOLZ; (*c*2) and (*c*3) enlargement of Fig. (*c*1).

visualized as $\log s = f(10^3/T)$ Arrhenius plots (593–973 K temperature range).

3. Structural results

3.1. Thermal behaviour

A powder sample of α-Pb_2BiVO_6 was heated to 703 K and kept at that temperature within the β stability domain. From 578 to 688 K, no modification of the X-ray diffraction lines was observed, while at 688 K the α form started to transform into the β form. The transformation was complete at 703 K. After air-quenching, the X-ray diffraction pattern observed at ambient temperature remained identical to the high-temperature typical β-phase pattern, Fig. 1. The high-temperature X-ray diffraction (HTXRD) run shows the successive modifications.

$$573 \xrightarrow[\text{slow heating}]{\alpha} 688 \xrightarrow[\text{slow heating}]{\beta} 703 \xrightarrow[\text{quenching}]{\beta} 293\ \text{K}$$

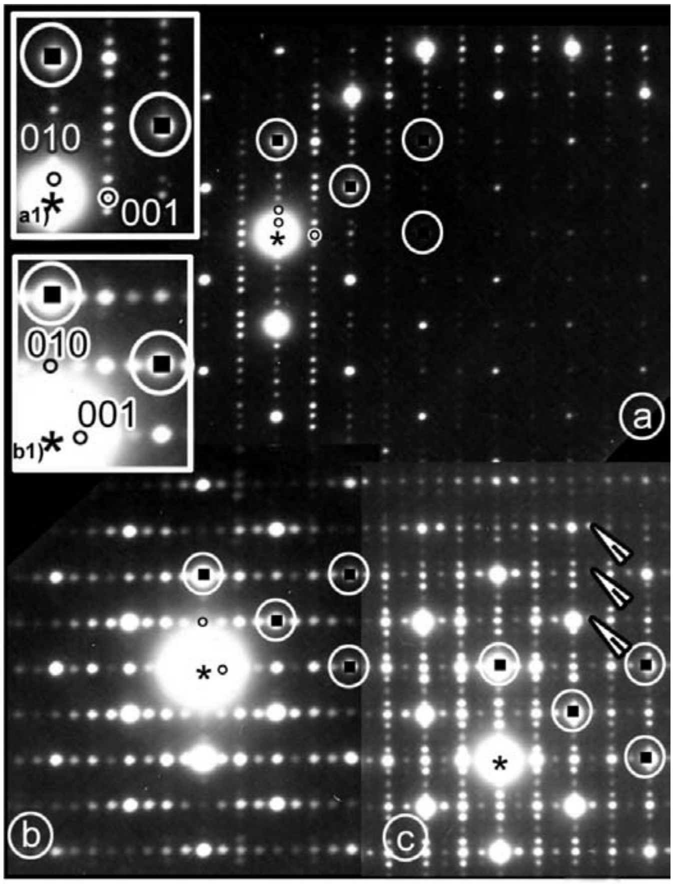

Figure 3
Crystal of the β synthesis: (*a*) *a* zone; (*a*1) enlargement of *a* zone; (*b*) *b* zone; (*b*1) enlargement of *b* zone; (*c*) zone *a* + *b*. White circles with black squares indicate the common spots of the three areas. White arrows point to the supplementary spots which appear on the [100] ZAP of the β phase according to the superposition.

However, under this temperature cycling the sample powder was not a single phase, neither at 703 K nor at 293 K. We systematically observed a few extra weak X-ray diffraction lines, characteristic of either the α or α' polymorphic forms (Labidi *et al.*, 2004).

3.2. TEM diffraction studies

3.2.1. β phase. As the β single-phase material cannot be obtained after the cooling process presented in the previous section, an electron-diffraction study of the β preparation was used in a search for the β lattice parameters. Reconstruction of the reciprocal space indicated a monoclinic cell: $a \simeq 15$, $b \simeq 23$, $c \simeq 7.5$ Å, $\beta \simeq 101^\circ$. No systematic extinction condition appeared, leaving a choice between $P2/m$, $P2$ and Pm as possible space groups. Figs. 2(*a*), (*b*) and (*c*) display the [010], [100] and [001] main zone axes, obtained with beam precession. The comparison of the zero-order Laue zone (ZOLZ) and first-order Laue zone (FOLZ) does not indicate any shift or periodicity difference along the [010] zone axis. This result is compatible with a partial extinction symbol $P-$ in the *International Tables for Crystallography* (Morniroli & Steeds, 1992). No glide plane is highlighted, in accordance with the reconstruction of the reciprocal network. Moreover, the b* axis shows a particular distribution of the diffraction intensities, which would suggest a modulated structure with a $\mathbf{q}$ modulation vector of ~ 0.25. This commensurate *versus* incommensurate character of the modulation was checked by exploring a larger zone of the reciprocal lattice network by TEM, Fig. 2. The second-order satellite reflections of +2 and −2 order were rigorously separated, indicating the incommensurate modulation character. This point will be detailed in §3.3.

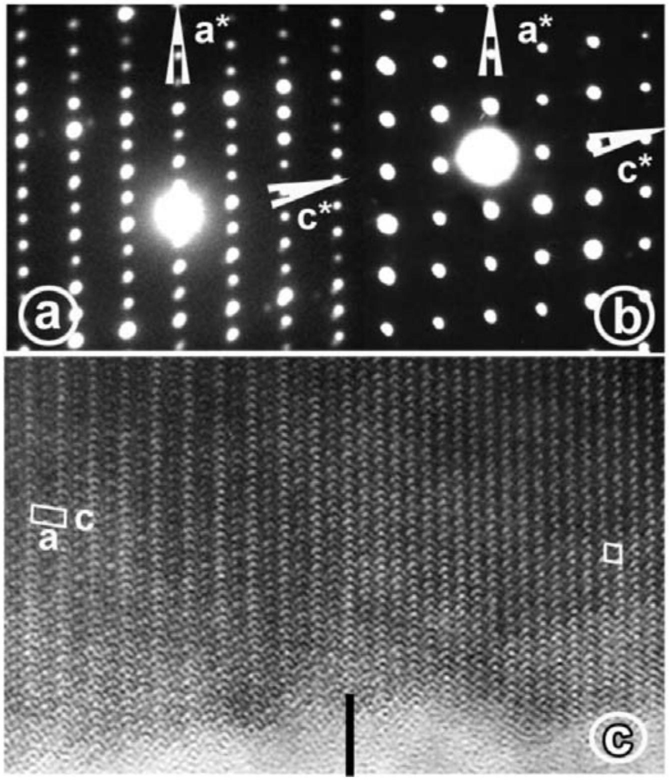

Figure 4
Coexistence of two areas on the same crystal. (*a*) EDP of zone *a*; (*b*) EDP of zone *b*; (*c*) corresponding image showing two different periodicities and no real frontier between them.

3.2.2. Illustration of the polymorphism: coexistence of several structures in the same crystallite. Three zones of the same crystallite appear in Fig. 3. The common spots are symbolized with black squares surrounded by white circles. The *a* zone is slightly disoriented compared with the other two. It is identified as the [100] zone-axis pattern (hereafter ZAP) of the β phase. The *b* area can be attributed to the [100] ZAP of the α' polymorph according to the distance measured on the diffraction pattern. The *c* zone consists of the superposition of these two previous areas, which leads to the presence of supplementary spots (white arrows) on the [100] ZAP of the β phase.

Two different zones can be observed on another crystal (Fig. 4). The first is the [010] ZAP of the β phase (Fig. 4*a*) and the second (Fig. 4*b*) reveals distances of $\sim 7.5 \times 7.3$ Å with $\beta \simeq 101^\circ$, which does not refer to any known parameter and suggests the existence of a novel phase. The corresponding image shows two zones with a different periodicity and the transition between these two areas is continuous without any defects, thus illustrating a similarity between these two polymorphs. A possible explanation of this second zone, which would imply a twofold superstructure along the *a* axis of the first zone, can possibly lie in slightly different orientations of the VO_4 tetrahedra, as already observed for α and δ polymorphs.

3.3. X-ray single-crystal data

Taking into account the information collected by high-temperature X-ray powder diffraction and transmission electron microscopy (TEM), we prepared single crystals of the β polymorph, as described in §2. A platelet-shape single crystal was selected out of the preparation, for the purpose of a structural investigation of β-Pb_2BiVO_6.

Initially, an orthorhombic C-cell, with lattice parameters a = 19.041 (3), b = 23.329 (4), c = 23.608 (2) Å, was proposed. However, even after applying an absorption correction (Sheldrick, 2004), the $R_{\rm int}$ value was as high as 0.205. On the other hand, the monoclinic cell values a = 15.0502 (7), b = 23.608 (1), c = 15.0629 (7) Å, β = 101.559 (2)° gave a reasonable $R_{\rm int}$ value of 0.0507. Moreover, this cell is consistent with conclusions made from TEM, except for the c parameter which is doubled.

A thorough examination of the reciprocal system suggests a possible explanation for this fact. We observed some reflections, $h = 2n + 1 \wedge l = 2n + 1$, which were not compatible with any conventional space group. Such reflections can follow on the superposition of two twin domains, DI and DII, related by 180° rotation around the [101] axis (Fig. 5). For each domain, the unit-cell parameters are a = 15.0502 (7), b = 23.608 (1), c = 7.55322 (5) Å, β = 101.56 (2)°, which confirms

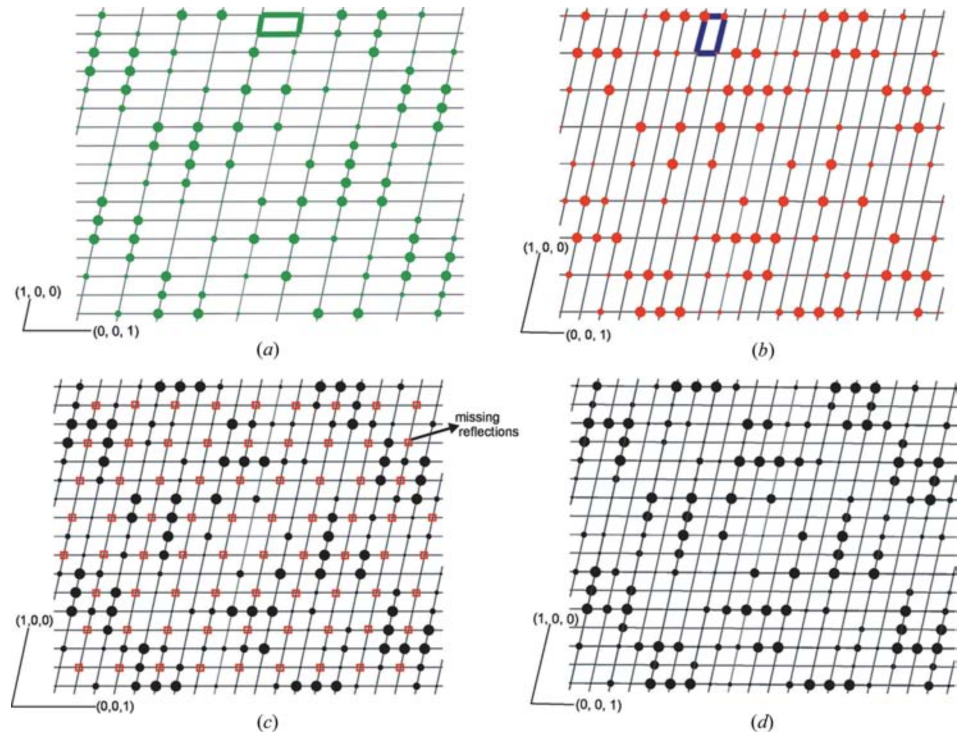

Figure 5
Reciprocal space of domain (*a*) I; (*b*) domain II; of unit-cell parameters $a = 15.0502$ (7), $b = 23.608$ (1), $c = 15.0629$ (7) Å, $\beta = 101.559$ (2)°; (*c*) observed pattern; (*d*) superposition of the domains I + II. Note that (*d*) ≡ (*c*).

the TEM results. The crystal zone studied by TEM is much smaller (just a few nanometers) compared with single-crystal X-ray diffraction (a few micrometers). Thus, it is more probable to observe both domains by X-ray diffraction.

The matrix was introduced describing the relation between basic vectors of two twin domains

$$\begin{pmatrix} \mathbf{a} \\ \mathbf{b} \\ \mathbf{c} \end{pmatrix}_{\rm II}. \qquad (1)$$

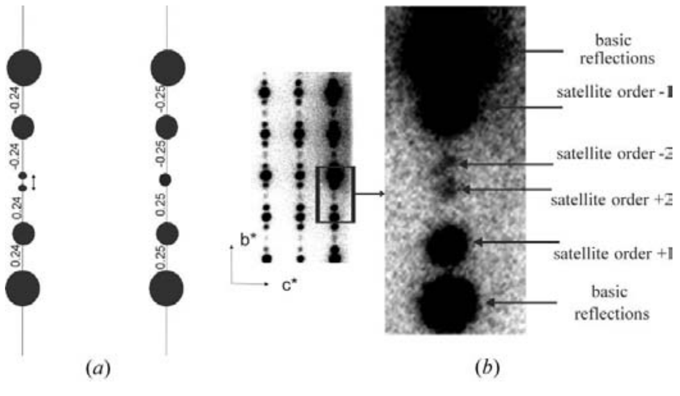

Figure 6
(*a*) Theoretical scheme illustrating the difference between commensurate (right part) and incommensurate (left part) modulation; (*b*) zoom of an experimental pattern clearly showing the incommensurate modulation.

The *JANA*2006 (Petricek *et al.*, 2006) software allows us to differentiate *a posteriori* reflections from domain I and domain II, as well as overlapping reflections of both domains.

As already noted in the TEM study, the structure is modulated. The same observations can be made on the X-ray data: reflections with $k = 4n$ along the b axis are very strong, corresponding to main reflections, the others being satellite reflections. In a first approximation, we could propose a basic unit cell (a, $b/4$, c), *i.e.* $a = 15.0501$ (5), $b = 5.9011$ (3), $c = 7.5322$ (5) Å, $\alpha = 90$, $\beta = 101.56$ (2), $\gamma = 90°$, and the modulation vector $\mathbf{q} = 0.25\mathbf{b}^*$. The 0.25 value has been refined to 0.2338 (3) using the *Nada* software (Schönleber *et al.*, 2001). The incommensurate modulation is visible by zooming in on an adequate zone of the reciprocal space observed by TEM, where separated satellites of the order 2 and −2 are presented (Fig. 6). The superspace (3 + 1)-dimensional approach was thus used to model the modulated structure of the β form.

3.3.1. Average structure. In the average structure [cell parameters $a = 15.0501$ (5), $b = 5.9011$ (3), $c = 7.5322$ (5) Å, $\alpha = 90$, $\beta = 101.56$ (2), $\gamma = 90°$], the space groups which are compatible with the extinctions observed on main reflections are $P2_1/m$ and $P2_1$ [only the single reflection 010 violates the extinction condition, with the ratio $1/\sigma(I) \simeq 5.6$]. After testing these two possibilities, $P2_1/m$ was retained for the refinement process. The program *SIR*2002 (Burla *et al.*, 2003) was used to identify the heavy-atom positions Pb, Bi and V in the basic unit cell, but the proposed solution was not satisfactory giving a high reliability factor ($R \simeq 0.28$). *SIR*2002 does not take this twinning into account to calculate the R factor. Considering the twinning effects (*i.e.* the fractional volume of the two domains; the reflections of the domains I, II and III), *JANA*2006 indicates the more satisfactory value $R \simeq 0.12$. When introducing the anisotropic displacement coefficients for the lead and bismuth heavy atoms, R decreases to 0.05. The principal difficulty is to identify the O-atom positions of the VO_4 tetrahedra. Both independent VO_4 groups have their central V atoms located at the mirror plane. A Fourier-difference map calculated in the vicinity (5 Å cube) of V1 was used to locate the surrounding O atoms. The projection along the [001] direction (see Fig. 7) shows that there are two clearly distinct VO_4 positions related by the mirror plane. The $V2O_4$ group similarly showed two groups both fitting the local crystallographic site symmetry approximately related by the twofold axis along the [1,0,−1] direction. Adding the oxygen atomic positions found on the difference-Fourier maps, the refinement of the main reflection dataset converged in a few cycles towards a reasonable value of $R \simeq 0.036$.

3.3.2. Modulated structure. The modulation of the structure is clearly shown on the (001) high-resolution image with the undulation of each layer. 2145 first-order satellites were observed, while only 41 second-order satellites out of 36 732 were regarded as observed but with an average ratio of $I/\sigma(I) \simeq 3.2$. Examination of the recorded photographs proved that these second-order satellites in fact belong to the background, illustrating a standard problem of CCD detectors, *i.e.* an undervaluation of the standard uncertainty value during the integration process. Consequently, we decided to consider only the first-order set of satellite reflections during the refinement process. In a TEM run, second-order satellites are very weak and thus difficult to observe in spite of an electron-matter interaction approximately 10^6 greater than with an X-ray source. The choice of a superspace group cannot be made by examining just the main reflections, and satellites have to be taken into account. The two possible superspace groups compatible with the three-dimensional parent space group found for the average structure are $P2_1/m(0\beta0)00$ and $P2_1/m(0\beta0)s0$. As a check of the systematic extinctions of the satellite reflections could not give a clear indication as to which superspace group is correct, refinements in both superspace groups were made. It led to the unambiguous conclusion that the $P2_1/m(0\beta0)s0$ group was the correct one.

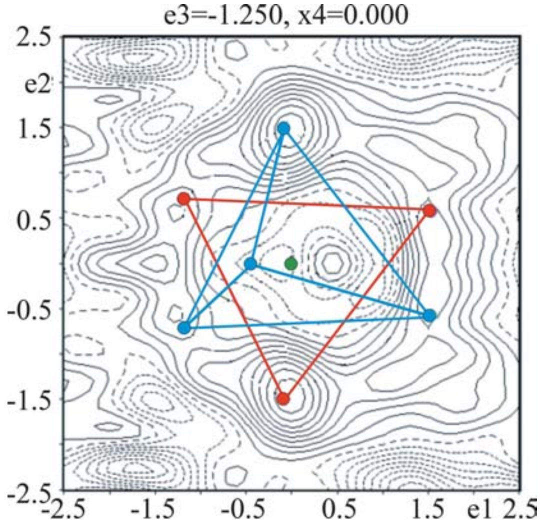

Figure 7
Difference-Fourier map around the V1 atom (in a cubic box of $2.5 \times 2.5 \times 2.5$ Å^3) to locate the surrounding O atoms and representation of the two tetrahedral configurations (contour 2 e Å^{-3}).

Atomic displacement modulations were introduced for all the atomic species and yielded encouraging R values of R[obs,main + sat] = 0.0670, R[obs,main] = 0.0373, R[obs,sat] = 0.1206. All atoms belonging to the O(Bi, Pb)$_4$ tetrahedra forming the double ribbons are affected by a displacement modulation which can be shaped as an undulated cord, Fig. 8.

Consequently, the interatomic distances are affected by this atomic displacement modulation function and they fluctuate according to the internal coordinate t. An example of the variation of the Bi1—O distances with t in the O(Bi, Pb)$_4$ tetrahedra is represented in Fig. 9, indicating an evolution from 2.25 to 2.50 Å.

Moreover, as already indicated, the environment of V1O$_4$ tetrahedra is disordered into two dominant positions related by the local mirror plane. Therefore, we introduced an occupation modulation on the V1O$_4$ rigid blocks. The harmonic model gives the occupation modulation represented in Fig. 10 for V1O$_4$ tetrahedra. One can clearly see that there are zones where the independent tetrahedron position is more than half occupied with a maximal occupancy at $\sim t = 0.44$ and a complementary region with the occupancy always smaller than half. One can attempt to describe this case using a crenel model. In *JANA*2006 the crenel function is defined by two parameters addressing the width of the crenel (Δ) and the centre of the crenel segment (x_{40}).

For the V1O$_4$ tetrahedron, the modulation function in the harmonic model reaches its maximum for t = 0.44, a value which corresponds to the central position of the crenel. However, an x_{40} origin must be given to define the crenel function (rather than a t_{40} one). By definition, we

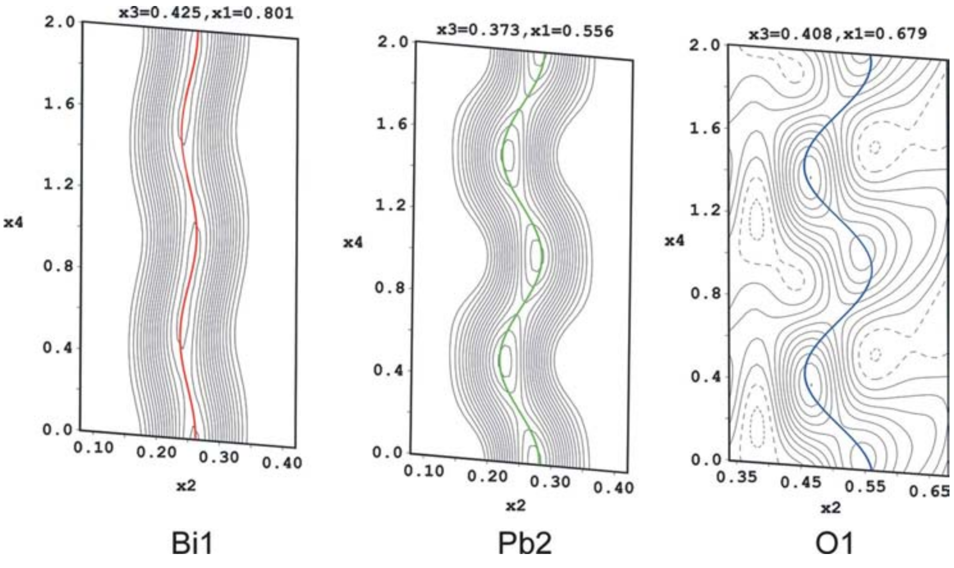

Figure 8
x_2–x_4 sections showing the electron density at the Bi1, Pb2 and O1 positions (contour: 25 e Å^{-3} for Bi1 and Pb2 and 2 e Å^{-3} for O1). The density map for O1 atom was made as a difference-Fourier map prepared from a model in which O1 was temporarily omitted.

Acta Cryst. (2009). B65, 416–425 Pascal Roussel et al. • Structure of β-Pb$_2$BiVO$_6$ 421

know that $x_4 = \mathbf{q}\cdot\mathbf{r} + t$. Then, for V1 at the special position (0,0.25,0), x_{40}(V1) = 0.2338 × 0.25 + 0.44 $\simeq$ 0.4985. We have to introduce a constraint such that when a site is completely filled, its symmetry is non-existent [the (average) mirror symmetry is lost so that a constraint must be added to avoid an overlapping of the various configurations]. The first tetrahedron is described by a crenel centred in x_{40} = 0.4985. Equivalent positions deduced from the superspace group $P2_1/m$ $(0\beta0)s0$ are (x_1, x_2, x_3, x_4) and (x_1, $-x_2$, x_3, $-x_4$). Consequently, the second configuration of the tetrahedron $V1O_4$ deduced from the first one is a crenel centred at $x_{40} = \frac{1}{2} -$ 0.4985 = 0.0015. The first tetrahedral position is determined in the interval [0.2485, 0.7485] and the second between [−0.2485, 0.2515], which both overlap on a short zone [0.2485, 0.2515] and also leave a second empty area on the space [0.7485, 0.7515]. To avoid these overlapping zones, we must impose the condition

$$t_{40}(2) = t_{40}(1) - \frac{1}{2} \tag{2}$$

(because the width of the crenel is 1/2). On the other hand, the symmetry operator gives

$$x_{40}(2) = \frac{1}{2} - x_{40}(1). \tag{3}$$

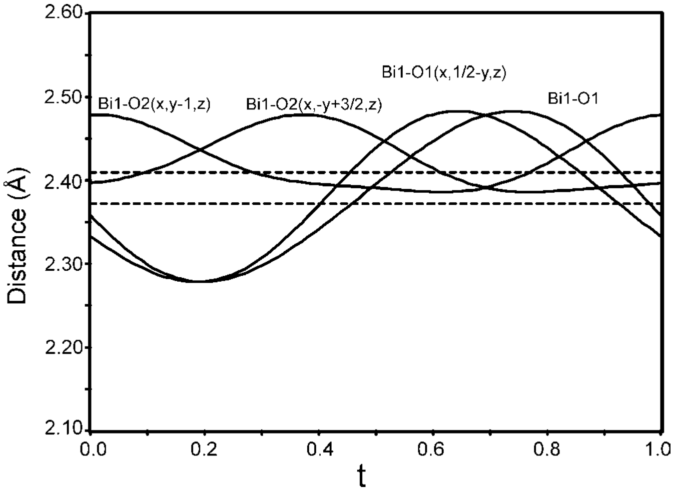

Figure 9
Bi1—O distances as a function of *t*.

We know that

$$x_{40}(1) = \mathbf{q}\cdot\mathbf{r}(1) + t_{40}(1) \text{ and } x_{40}(2) = \mathbf{q}\cdot\mathbf{r}(2) + t_{40}(2), \text{ thus}$$

$$\mathbf{q}\cdot\mathbf{r}(2) + t_{40}(2) = \frac{1}{2} - \mathbf{q}\cdot\mathbf{r}(1) - t_{40}(1). \tag{4}$$

Using (2), we obtain

$$\mathbf{q}\cdot\mathbf{r}(2) + t_{40}(1) - \frac{1}{2} = \frac{1}{2} - \mathbf{q}\cdot\mathbf{r}(1) - t_{40}(1), \text{ thus}$$

$$t_{40}(1) = \frac{1}{2} - \frac{1}{2}[\mathbf{q}\cdot\mathbf{r}(1) + \mathbf{q}\cdot\mathbf{r}(2)]. \tag{5}$$

The modulation wavevector possesses a unique component (β) along the b^* axis from where it follows that

$$\begin{aligned}[\mathbf{q}\cdot\mathbf{r}(1) + \mathbf{q}\cdot\mathbf{r}(2)] &= [\beta\cdot y(1) + \beta\cdot y(2)] \\ &= [\beta\cdot y(1) + \frac{1}{2}\beta - \beta\cdot y(1)]\end{aligned} \tag{6}$$

with

$$y(2) = \frac{1}{2} - y(1)\ \beta\cdot y(2) = \frac{1}{2}\beta - \beta\cdot y(1), \text{ thus}$$

$$[\mathbf{q}\cdot\mathbf{r}(1) + \mathbf{q}\cdot\mathbf{r}(2)] = \frac{1}{2}\beta. \tag{7}$$

Finally, the equation

$$t_{40}(1) = \frac{1}{2} - \frac{1}{4}\beta \tag{8}$$

must be introduced for the $V1O_4$ tetrahedron.

The case of the $V2O_4$ tetrahedron is similar: two positions are connected by the mirror *m*. The occupation is maximum at *t* = 0.70 for the first position of the tetrahedron $V2O_4$, *i.e.* as for $V1O_4$, $x_{40} = \mathbf{q}\cdot\mathbf{r} + t$ = 0.2338 × 0.25 + 0.70 = 0.7585 and for the second position, x_{40} = 0.2338 × 0.25 + 0.20 = 0.2585. The mirror restricts the x_{40} positions to 0.75 and 0.25. After the introduction of these equations into *JANA*2006, the crenel model gives the values: *R*[obs, main + sat] = 0.0599, *R*[obs, main] = 0.0381, *R*[obs, sat] = 0.0991 for 128 parameters, whereas the harmonic model gives *R*[obs, main + sat] = 0.0598, *R*[obs, main] = 0.0381, *R*[obs, sat] = 0.0982 for 131 parameters. The crenel model is simpler to describe than the harmonic model and it was thus retained for the remainder of the refinement. As indicated above, the atomic environment is affected by an atomic displacement modulation varying with *t*. Since the neighbouring of the affected atoms is modified, it is quite natural to introduce a displacement parameter modulation. Once it was introduced, the refinement converged towards: $R_{\rm final}$ = 0.0362, $R_{\rm main}$ = 0.0307, $R_{\rm satellites}$ = 0.0459. The O atoms in the VO_4 group were refined

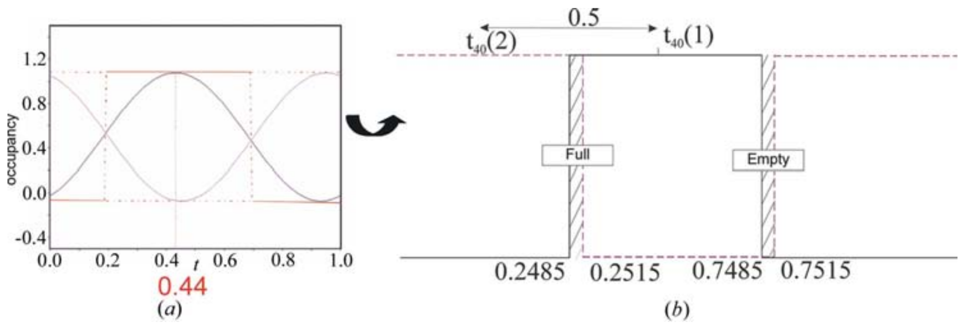

(*a*) (*b*)

Figure 10
(*a*) Variation of the occupation factor *versus t* for VO_4 rigid bodies (harmonic model); (*b*) representation of this variation by a simple crenel function of width Δ = 0.5.

with isotropic displacement parameters. Neither the model with anisotropic ADPs for these O atoms nor TLS tensors gives a significant improvement of the already low goodness-of-fit (1.07). This is a consequence of the fact that the actual scattering power of these split O atoms is a very small fraction of that of the structure. The main crystallographic data are summarized in Table 2.

3.4. Discussion

The structures of the α (Radosavljevic Evans *et al.*, 2001), β, δ (Radosavljevic Evans *et al.*, 2002) and also α' (Labidi *et al.*, 2004) and δ' (Labidi *et al.*, 2005) polymorphic forms of Pb_2BiVO_6 resulting from the manganese and phosphorus substitutions for V were solved from single crystal data. Now it is possible to carry out a structural comparison in order to understand the mechanism of the temperature-driven transition. For example, along the elongation axis of the $(O_2Bi_2Pb_4)_\infty$ ribbons, *i.e.* the b_β axis, the matrix relation between the α and β unit cells (β in the three-dimensional approximation) can be written as

$$\begin{pmatrix}\mathbf{a}\\ \mathbf{b}\\ \mathbf{c}\end{pmatrix}_\beta = \begin{pmatrix}-2 & 0 & 0\\ 0 & -4 & 0\\ \frac{1}{4} & 0 & \frac{1}{4}\end{pmatrix}\begin{pmatrix}\mathbf{a}\\ \mathbf{b}\\ \mathbf{c}\end{pmatrix}_\alpha . \qquad (9)$$

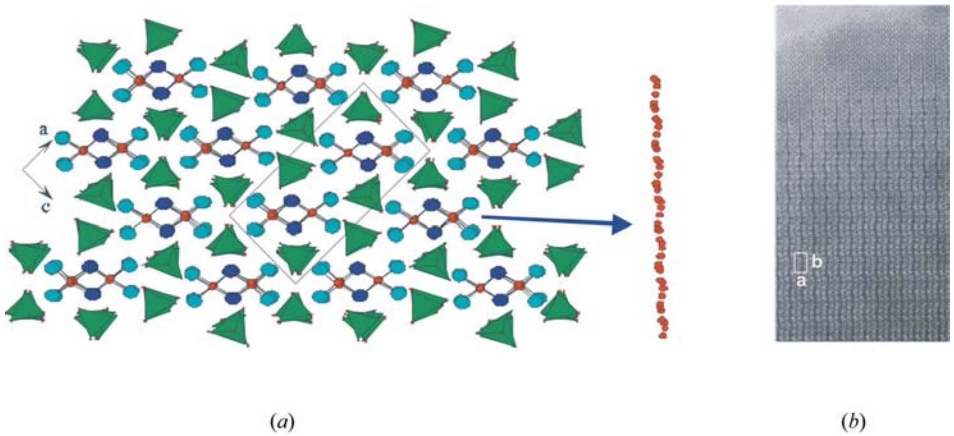

(*a*) (*b*)

Figure 11
(*a*) Projection along [010] of the structure and O2 modulated position (undulated cord) in $O_2Bi_2Pb_4$.

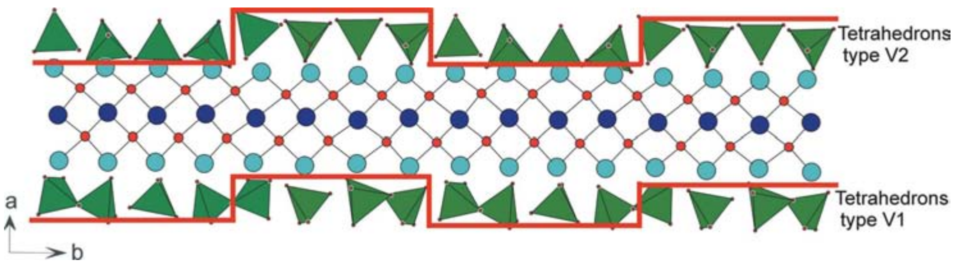

Figure 12
$O_2Bi_2Pb_4$ chains surrounded by VO_4 tetrahedra drawing the crenel function.

As for the α phase, the β-Pb_2BiVO_6 structure can be described as being built from O(Bi, Pb)$_4$ tetrahedral units which, by sharing Bi–Bi edges form $O_2Bi_2Pb_4$ dimers, which themselves share Bi–Pb edges to form two-dimensional infinite ribbons parallel to the b axis. The O2 atoms located at the centre of these OBi_2Pb_2 tetrahedra are affected by a modulated displacement and draw an undulated cord represented schematically, Fig. 11(*a*). This undulation is also clearly observed on the high-resolution TEM images, Fig. 11(*b*).

Each one of these ribbons is surrounded by six VO_4 tetrahedra, whose orientations are obtained by the refinement of a crenel function, *i.e.* showing a succession of four tetrahedra with partial occupancies, Fig. 12. The structural characteristic common to all these polymorphic phases is the infinite ribbon $O_2Bi_2Pb_4$ surrounded by six VO_4 tetrahedra, and the main difference appears to be the orientation of the tetrahedra VO_4 around these dimer ribbons.

The arrangement of the tetrahedra makes it possible to propose a representation in sequences of two tetrahedron blocks in order to compare the structures investigated so far, *i.e.* α, β, δ and δ' phases. A succession of four tetrahedra is found in the β structure: indeed, oriented in such a way that the Pb atoms are observed alternating at the corners or the edges of tetrahedra influenced by the crenel refinement. On the other side of the ribbon, a pair of VO_4 pointing corner against corner (with respect to the standard α-phase structure) are associated with two other vanadates, thus showing an overall set of four VO_4 units, *i.e.* V2 type in the crenel function representing the β structure model.

An overall scheme can be understood starting from these three crystalline forms at ambient temperature. The room-temperature stabilized β form can thus be described by an assembly of tetrahedra, which is seen in both α and β' forms. Although the sequence of transitions observed upon heating is $\alpha \rightarrow \beta \rightarrow \delta$, on cooling the δ' phase is obtained only in the case of the $Pb_2BiV_{1-x}P_xO_6$ solid solution, with $x \geq 0.15$ (Labidi *et al.*, 2005).

3.4.1. Comparison of α, β and δ structural types. In the α-Pb_2BiVO_6 structure, two pairs of VO_4 are seen on both parts of the central ribbon, each pair with its specific orientation, and being shifted along the ribbon elongation axis (thickness of half a OPb_2Bi_2 tetrahedron). The α to β transition mechanism mainly concerns the VO_4 entities: in this

Table 3
Electrical characteristics (E_a, eV) and σ_T (S cm^{-1}) of α-, β- and δ-$Pb_2BiV_{1-x}M_xO_{6\pm y}$ (M = P, Mn, Cr, x = 0.06).

Polymorph E_a (eV)/σ_T (S cm^{-1})	α		β		δ	
	E_a	$\sigma_{623\ \mathrm{K}}$	E_a	$\sigma_{693\ \mathrm{K}}$	E_a	$\alpha^{963\ \mathrm{K}}$
$Pb_2BiV_{0.94}Cr_{0.06}O_{6\pm y}$	1.44	7.9×10^{-8}	1.41	7.9×10^{-7}	1.61	1.6×10^{-3}
$Pb_2BiV_{0.94}Mn_{0.06}O_{6\pm y}$	1.12	7.9×10^{-7}	0.60	5.0×10^{-6}	1.55	1.3×10^{-3}
$Pb_2BiV_{0.94}P_{0.06}O_6$	1.02	1.2×10^{-7}	0.28	2.5×10^{-7}	1.58	1.2×10^{-4}

averaged representation of the β polymorph a sequence of four vanadate entities is identified on both sides (Fig. 12), alternatively oriented head-to-tail from one set to another on both sides of the ribbon (V1 and V2 types). Among many attempts to modify the overall transition sequence, the P for V substitution (Labidi *et al.*, 2005) shows a simplification of the mother phase transition scheme: with a 10% substitution rate, the intermediate decomposition of δ no longer occurs; at 15%, α goes directly to δ on heating, while on cooling δ yields a new related δ′ polymorph identified from an extra set of weak diffraction peaks at room temperature. At 25%, we only see δ′ to δ on heating, which is reversed on cooling; single crystals of the δ′ phase have been prepared. The structure has been determined as orthorhombic, *Pbca*, with a lattice constant *b* doubled from the δ related structure. The overall transition mechanism can be understood by including δ′ in the previous comparison: in the δ′ structure, two different sets of VO_4 pairs with their own orientations can be seen at the same level on both sides of the central ribbon; when going to δ, only one identical set of two VO_4 pairs characterizes this high-temperature polymorph.

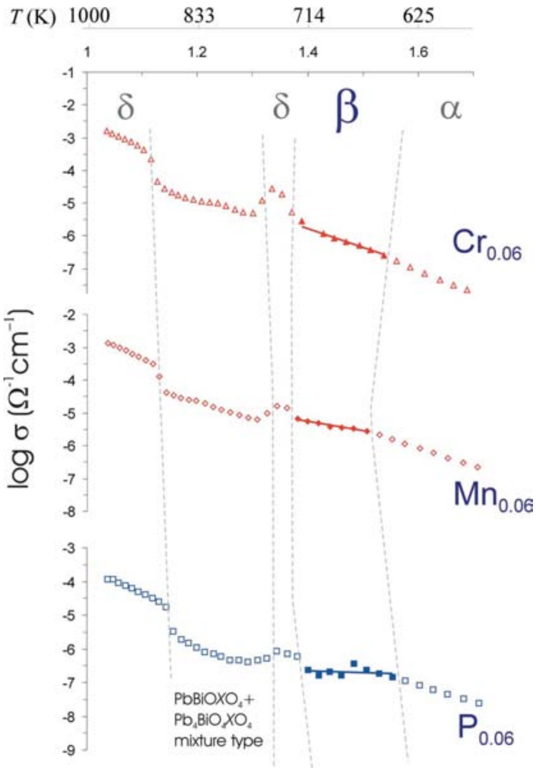

Figure 13
Initial heating Arrhenius plots for $Pb_2BiV_{0.94}M_{0.06}O_{6\pm y}$ (M = Cr, Mn, P) materials.

4. Conduction properties

Arrhenius plots obtained from conductivity measurements, conducted on Pb_2BiVO_6 as well as related solid solution compositions, have been previously reported (Mizrahi, Wignacourt *et al.*, 1995; Labidi *et al.*, 2005). On the basis of their (powder) thermal behaviour, and taking into account the logical difference in the temperature of transitions observed through various techniques, *i.e.* a difference in heating–cooling rates, every single part of these plots has been associated with a specific single phase (or intermediate decomposition mixture), in agreement with the general transformation scheme

$$\alpha \rightarrow \beta \rightarrow \delta \rightarrow (\gamma \text{ mixture}) \rightarrow \delta.$$

In fact, during the initial investigation of Pb_2BiVO_6 (Mizrahi, Wignacourt *et al.*, 1995), the $\alpha \rightarrow \beta$ transformation was characterized by a slight decrease of the conductivity level, while the subsequent intermediate formation of the δ variety was unsuspected.

Fig. 13 shows the heating part of the Arrhenius plots corresponding to three homologous materials, $Pb_2BiV_{0.94}M_{0.06}O_{6\pm y}$ (M = Cr, Mn, P). α, β (at least for Cr- and Mn-based samples) and δ varieties are characterized by linear evolution domains. The α and β varieties are distinguished by their specific activation energy, hereafter E_a, and we can easily conclude that $E_{a\beta} < E_{a\alpha}$. The better conductivity of the δ form allow the transitory to form and its high-temperature stable state to be distinguished.

Characteristic electrical properties values (conductivities at specific temperatures and corresponding activation energies) are given in Table 3. The dispersion of the measurement data limits the reliability of E_a for the P-substituted β form, whereas E_a was impossible to determine for the δ intermediate forms owing to their narrow stability domains *versus* temperature. The best conductivity at low temperature (α or β variety) is observed for the Mn-based material, whereas the δ-Cr substituted phase becomes the best conducting composition when the temperature increases to the maximum possible for material stability. For each examined material, the activation energy of the β phase is weaker than that observed for the α or β phases.

5. Conclusions

The Pb_2BiVO_6 β phase has been successfully preserved at room temperature under a specific heating–cooling cycle, consisting of heating a powder sample until the direct phase transition $\alpha \rightarrow \beta$ was completed; the sample was then annealed in the β domain, and finally a slow cooling process brought it down to room temperature. A similar cycle was successfully applied to single crystals. The structure of β-

Pb_2BiVO_6 was solved from X-ray diffraction single-crystal data in a (3 + 1)-dimensional superspace approach with an incommensurate modulation; complementary structural investigations of a β-Pb_2BiVO_6 powder sample by TEM diffraction studies confirmed the lattice and space-group settings.

The structural relationship between the α-, β- and δ-Pb_2BiVO_6 polymorphs, and their related α' and δ'-$Pb_2Bi(V_{1-x}M_x)O_6$-substituted forms has been explored, and the transition mechanism is found to mainly result from reorientations of VO_4 entities with temperature: in α-Pb_2BiVO_6, two pairs of VO_4 are surrounding the central ribbon, each pair showing its own orientation and being shifted along the ribbon-elongation axis; in the averaged representation of the β-Pb_2BiVO_6 polymorph, a set of four vanadate entities is seen on both sides of the backbone ribbon, alternatively oriented head-to-tail. In the δ'-Pb_2BiVO_6 structure, two different sets of VO_4 pairs having their own orientations can be seen without any shift on both sides of the central ribbon, while in δ-Pb_2BiVO_6, only one single set of two VO_4 is seen in the high-temperature polymorph.

Ionic conductivity *versus* temperature has been measured in this new β-Pb_2BiVO_6 phase as well as in related solid solutions.

The ‘Fonds Européen de Développement Régional (FEDER)’, ‘CNRS’, ‘Région Nord Pas-de-Calais’ and ‘Ministère de l’Education Nationale de l’Enseignement Supérieur et de la Recherche’ are acknowledged for funding the X-ray diffractometers. The authors are also grateful to L. Burylo and N. Djelal for their help with the X-ray diffraction and thermal analyses. The development of the *JANA*2006 program is supported by the Czech Science Foundation No. 202/06/0757.

References

Burla, M. C., Camalli, M., Carrozzini, B., Cascarano, G. L., Giacovazzo, C., Polidori, G. & Spagna, R. (2003). *J. Appl. Cryst.* **36**, 1103.

Giraud, S., Mizrahi, A., Drache, M., Conflant, P., Wignacourt, J. P. & Steinfink, H. (2001). *Solid State Sci.* **3**, 593–602.

Giraud, S., Wignacourt, J. P., Drache, M., Nowogrocki, G. & Steinfink, H. (1999). *J. Solid State Chem.* **142**, 80–88.

Labidi, O., Roussel, P., Huve, M., Drache, M., Conflant, P. & Wignacourt, J. P. (2005). *J. Solid State Chem.* **178**, 2247–2255.

Labidi, O., Wignacourt, J. P., Roussel, P., Drache, M., Conflant, P. & Steinfink, H. (2004). *Solid State Sci.* **6**, 783–790.

Mizrahi, A. (1996). PhD Thesis, UST Lille, France.

Mizrahi, A., Huve, M., Conflant, P., Drache, M. & Wignacourt, J. P. (1995). Proceedings XXIth JEEP, p. 272.

Mizrahi, A., Wignacourt, J. P., Drache, M. & Conflant, P. (1995). *J. Mater. Chem.* **5**, 901–904.

Mizrahi, A., Wignacourt, J. P. & Steinfink, H. (1997). *J. Solid State Chem.* **133**, 516–521.

Morniroli, J. P. & Steeds, J. W. (1992). *Ultramicroscopy*, **45**, 219–239.

Petricek, V., Dusek, M. & Palatinus, L. (2006). *JANA*2006. Institute of Physics, Praha, Czech Republic.

Radosavljevic Evans, I., Evans, J. S. O. & Howard, J. A. K. (2002). *J. Mater. Chem.* **12**, 2648–2652.

Radosavljevic Evans, I., Howard, J. A. K., Withers, R. L. & Evans, J. S. O. (2001). *Chem. Commun.* **19**, 1984–1985.

Schönleber, A., Meyer, M. & Chapuis, G. (2001). *J. Appl. Cryst.* **34**, 777–779.

Sheldrick, G. M. (2004). *SADABS* 2004/1. University of Göttingen, Germany.